JOURNAL OF Materials CHEMISTRY

Zeolite syntheses using linear diquats of varying length in fluoride media. The synthesis of ITQ-8, ITQ-10, ITQ-14 and high silica Nu-87†

M. J. Díaz-Cabañas,[a] M. A. Camblor,*[a,b] Z. Liu,[c] T. Ohsuna[d] and O. Terasaki[c,e]

[a]*Instituto de Tecnología Química (CSIC-UPV), Avda. Los Naranjos s/n, 46022 Valencia, Spain*
[b]*Industrias Químicas del Ebro, Pol. Malpica, Calle D, n° 97, 50057 Zaragoza, Spain. E-mail: macamblor@iqe.es*
[c]*CREST, Japan Science and Technology Corporation, Tohoku University, Sendai 980-8578, Japan*
[d]*Institute for Materials Research, Tohoku University, Sendai 980-8577, Japan*
[e]*Department of Physics and CIR, Tohoku University, Sendai 980-8578, Japan*

Received 15th June 2001, Accepted 30th October 2001
First published as an Advance Article on the web 4th January 2002

Three linear diquats of different lengths (consisting of two quinuclidinium groups linked by a chain of 8, 6 or 4 methylene groups) have been used as structure directing agents in the synthesis of silica zeolites in the presence of fluoride anions. Phase selectivity changes induced by changes in the concentration of the crystallizing mixture or by the addition of Al have been investigated. For the longest diquat only Beta and ZSM-12 were detected by X ray diffraction in the product, with Beta being favoured at high concentrations, low temperatures and short crystallization times. As the length of the chain decreases other phases, in addition to Beta and ZSM-12, appear: ZSM-5 (for the diquat of intermediate length) and ITQ-8, ITQ-10 and ITQ-14 (for the shortest diquat). ITQ-8 is most likely a layered silicate, while ITQ-10 and ITQ-14 are stable zeolites with intergrown structures related to the zeolite Beta family. Notably, ITQ-14 was found to consist of crystallites with the so far hypothetical "structure C" overgrown on standard zeolite Beta crystals. The phase selectivity effect of introducing Al into the gel is generally similar to the effect of decreasing its water content. However, with the longest diquat a different zeolite, Nu-87, crystallized in the presence of Al in a wide range of Si/Al ratios (25–200) but not for pure silica compositions or for the shortest diquats.

Introduction

In the synthesis of zeolites with intermediate to high Si/Al ratios the structure directing effect of organic cations are crucially important, but still poorly understood. These cations were formerly known as templates but now the term "Structure Directing Agent" or SDA is taking over because in the synthesis of zeolites there are very few examples of a proper "template" effect, which implies a close geometrical fit and a specific interaction between the cation and the framework it directs to.[1] The understanding of the structure directing effect of the SDA is difficult for several reasons, including that very frequently the phase selectivity of the crystallization depends on "inorganic conditions" as much as on the specific organic SDA being used.[2] One important parameter controlling the phase selectivity is the degree of dilution of the synthesis mixture, which was first noticed by Gies in the synthesis of clathrasils in the presence of neutral amines,[3] and recently studied by us in the synthesis of zeolites in fluoride media using quaternary ammonium cations.[4] The presence of fluoride itself in the crystallizing mixture has been shown to have an effect in the phase selectivity of the crystallization of microporous materials.[5]

One line of research is the systematic variation of the SDA, trying to understand which of its features is of importance in determining the phase selectivity of the crystallization. In this work we chose linear diquats (*i.e.* organic compounds with two positive charges) to search for phase selectivity effects related to the length separating the charges during the synthesis of zeolites in fluoride media. Several studies had focused before on the use of linear diquats[6] and polymeric cations[7,8] in the synthesis of zeolites in hydroxide media, finding in some cases interesting relations between the length of the organic and/or of its charge separation and the framework of the zeolite that crystallizes (either in terms of unit cell dimensions[7] or in terms of the separation between side pockets).[6] However, in the presence of fluoride this anion typically counterbalances the positive charge of the SDA and tends to end up occluded inside small cages (with a claimed structure direction effect of its own),[5,9] so it could be argued that the separation between the organic charges might perhaps influence the structure formed more strongly in fluoride than in hydroxide media. The SDA used in this study are 1,8-diquinuclidiniumoctane C_8H_{16}-$(C_7H_{13}N^+)_2$, 1,6-diquinuclidiniumhexane $C_6H_{12}(C_7H_{13}N^+)_2$, and 1,4-diquinuclidiniumbutane $C_4H_8(C_7H_{13}N^+)_2$, and will be referred for short as M_nBQ^{2+}, where n is the number of methylene groups in the lineal chain separating the quinuclidinium moieties.

Experimental

Synthesis of the diquats

The SDAs were prepared by reaction of the appropriate 1,*n*-dibromoalkane with quinuclidine in a molar ratio of 4 to 9

†Electronic supplementary information (ESI) available: ^1H and ^{13}C NMR spectra of M_nBQ^{2+} linear diquats and XRD pattern of the "unknown material" from Table 4. See http://www.rsc.org/suppdata/jm/b1/b105273j/

using ethanol as solvent. The reaction was carried at room temperature for three days with stirring. Then, the solvent was removed by evaporation under vacuum and the resulting solid was washed with ethyl acetate and diethyl ether. ^{1}H and ^{13}C NMR in D_2O (see ESI†) and chemical analysis confirmed that the products were the corresponding M_nBQ^{2+} cations in the dibromide dihydrated form. The dibromides were then exchanged to the dihydroxide forms in water solution using an OH^- resin (Dowex-1). The extent of exchange was always above 90%. In what follows, the molar amount of $M_nBQ(OH)_2$ in the synthesis mixtures is based on the titrated amount of hydroxide.

Zeolite synthesis

Tetraethylorthosilicate (TEOS, Merck) was added to an aqueous solution of $M_nBQ(OH)_2$ and then the mixture was stirred at room temperature for an extended period of time in order to allow complete evaporation of the ethanol produced plus the water needed to reach the desired final composition. In some cases, Al isopropoxide was also added and cohydrolyzed with TEOS. Then, the required amount of HF (aq. solution recently titrated, typically 45–48 wt%) was added and the mixture homogeneized by hand stirring. The mixture was poured into several Teflon lined stainless steel autoclaves and these were heated at the required crystallization temperature (135, 150 or 175 °C) while rotated (60 rpm). The gel composition was

$$SiO_2 : x\ Al_2O_3 : 0.25\ M_nBQ(OH)_2 : 0.50\ HF : w\ H_2O$$

and x was varied between 0 and 0.05 and w between 1.5 and 15. After cooling the autoclaves, the contents were filtered and the recovered solid was washed with water and dried at 100 °C.

Characterization

Phase purity and crystallinity were determined by conventional powder X-ray diffraction (XRD) using a Philips X'Pert diffractometer (Cu K_α radiation provided by a curved Cu monochromator). *In situ* high temperature XRD experiments were performed using an Anton Paar HTK16 camera provided with a 1 mm thick Pt filament and installed in a second goniometer of the same diffractometer. C, H and N contents were determined with a Carlo Erba 1106 elemental analyzer. The Al content was determined by atomic absorption. The fluoride content was determined using an ion-selective electrode connected to a Mettler Toledo 355 ion analyzer after dissolution of the as-made solids by a standard procedure.[10] Thermogravimetric analyses were performed on a NETZSCH STA 409 EP thermal analyzer in the range 293–1073 K with *ca.* 0.0200 g of sample, a heating rate of 10 K min^{-1} and an air flow of 6 l h^{-1}. The ^{29}Si MAS NMR spectra of the solids were recorded on a Varian VXR 400SWB spectrometer with a spinning rate of 5.5 kHz at a ^{29}Si frequency of 79.459 MHz, with a 55.4° pulse length of 4.0 μs and a recycle delay of 60 s. ^{29}Si chemical shifts are reported relative to TMS. N_2 adsorption/desorption and Ar adsorption experiments were undertaken isothermally at 77 and 85 K, respectively, using an automatic ASAP 2000 Micromeritics apparatus. The infrared spectra were recorded using a Nicolet 710 FTIR spectrometer. For the characterization of the acidity of the calcined materials the OH stretching and the pyridine skeletal vibration regions were monitored using self-supported wafers. Spectra were obtained at room temperature after outgassing the materials overnight at 400 °C under dynamic vacuum of 10^{-3} Pa and after adsorption of pyridine at room temperature and outgassing under vacuum at 250, 350 and 400 °C, respectively. Finally, crystal size and morphology were monitored by scanning electron microscopy (SEM) using a JEOL JSM-6300 microscope. For TEM observations, a JEM-4000EX with an accelerate voltage of 400 kV was used and the samples were first dispersed in ethanol by ultrasonication and then dropped on carbon microgrids.

Results and discussion

M_8BQ^{2+} as SDA

For pure silica compositions only two zeolites were detected in the final solids by XRD, Beta and ZSM-12 (Table 1). Both are large pore zeolites (with openings formed by rings of 12 tetrahedra, 12MR) but the channel system is monodimensional in ZSM-12 while it is three-dimensional in zeolite Beta. The first synthesis of pure silica Beta, with[11] or without seeds,[12] was not possible until very recently. However, we have now synthesized this phase using a large number of different organic SDAs, always in the fluoride medium and at medium to high concentrations of the reacting mixture.[4,13]

The results summarized in Table 1 show how the phase selectivity of the crystallization depends on the concentration of the gel (H_2O/SiO_2 ratio), on the temperature and on the crystallization time. As frequently observed in fluoride medium,[4] the phase with higher framework density (ZSM-12) is obtained for more dilute mixtures, higher crystallization temperatures and longer crystallization times. Only for two sets of conditions in Table 1 (high temperature with medium H_2O/SiO_2 ratio and low temperature with high H_2O/SiO_2 ratio) do both phases compete and an Ostwald ripening transformation, though very slow, is observed.

At a first glance this could be rationalized as a kinetic control by which zeolite Beta, assumed as a metastable phase with respect to ZSM-12, crystallized only under conditions of high supersaturation with a nucleation rate faster for Beta than for ZSM-12 under these conditions. Within this view, the higher stability of ZSM-12 would be supported by its crystallization at higher temperature and mostly by the observed Ostwald ripening transformation, which is slow probably because of the very low solubility of both phases in the synthesis conditions (yields are typically above 95%, based on silica).

However, when the as-made zeolite synthesized using M_8BQ^{2+} is used as the only silica source under synthesis conditions in which the opposite zeolite is obtained when TEOS is used, we only observed some transformation of ZSM-12 into Beta but not the opposite.[4] This raises some questions about the relative stability of ZSM-12 and Beta in the synthesis medium, suggesting that there is not a single answer: it does not depend only on the SiO_2 framework and its interaction with the guest species (organic cation and fluoride anion) but also on the concentration of the medium. We have recently observed that in zeolite synthesis using

Table 1 Zeolite synthesis results for pure silica compositions using M_8BQ^{2+} as SDA[a]

	Temperature/°C		
H_2O/SiO_2	175	150	135
4	Beta (2)	Beta (2)	Beta + am. (3)
	Beta (8)	Beta (8)	Beta (9)
7.5	Beta (4)	Beta (4)	Beta (4)
	Beta (12)	Beta (12)	Beta (12)
10	Beta (3)		
	Beta (28)		
12.5	Beta(3)		
	Beta (+ZSM-12) (28)		
15	ZSM-12 (7)	ZSM-12 + am. (7)	Beta + ZSM-12 (20)
	ZSM-12 (14)	ZSM-12 (14)	ZSM-12 (42)

[a]The numbers in parentheses correspond to the crystallization time in days; am. = amorphous solid.

benzylquinuclidinium the phase selectivity, which also changes with the H_2O/SiO_2 ratio, strongly depends on the concentration of the SDA, favoring the less dense phase at higher SDA concentrations.[14] The same appears to be true also here and one wonders if this may just be due to the fact that, normally, a less dense zeolite occludes a larger concentration of SDA cations (and F anions). The chemical composition of Beta and ZSM-12 zeolites prepared using M_8BQ^{2+} are listed in Table 2. The chemical data show that, indeed, the organic and fluoride content in Beta is more than twice that in ZSM-12. Another conclusion from the data listed in Table 2 is that the amount of fluoride occluded in both zeolites affords complete charge balance of the two charges introduced by each SDA diquat. The cation appears to be essentially intact in the zeolites, since in both cases the C/N ratio is 10.9, very close to the value in the SDA (11).

When Al is introduced into the synthesis gel a change in the phase selectivity is observed (Table 3). This is rather common in zeolite synthesis and we have observed that increasing the concentration of aluminum frequently has the same effect as decreasing the H_2O/SiO_2 ratio.[4] However, this is not so with M_8BQ^{2+}, since in this case the product obtained is zeolite Nu-87, a two-dimensional 10MR zeolite, rather than zeolite Beta.

Nu-87 is an interesting zeolite with a structure (code NES) in which adjacent 10MR channels are connected through 12MR cavities which are accessible through 10MR windows.[15] Due to this peculiar pore system and to the strong acidity found in H-Nu-87, this is an attractive material from the viewpoint of catalysis.[16] It is interesting that zeolite Nu-87 can be obtained in a rather large range of Si/Al ratios (at least 25–200) using this M_8BQ^{2+} in fluoride medium. The typical synthesis of Nu-87 in hydroxide medium makes use of similar SDAs (linear bistrimethylammonium diquats with chains of 8–12 methylenes) but the Si/Al ratios are smaller than 50.[17] This shows the suitability of the fluoride route for the synthesis of very high silica zeolites, a fact that may be related, at least in part, to the lower concentration of defects in the materials prepared by this route.[4] However, zeolite SSZ-37,[18] which is isomorphous to Nu-87, may be prepared in hydroxide medium with higher Si/Al ratios than Nu-87 and even as a pure silica phase when seeds are used. We note here that attempts to synthesize pure silica Nu-87 using M_8BQ^{2+} by adding Nu-87 seeds were unsuccessful and ZSM-12 crystallized instead (Table 3). Given that Nu-87 is less dense than ZSM-12 we tried also to slightly decrease the water to silica ratio from 15 to 12.5. Zeolite Beta crystallized in this case (Table 3), again showing the effect of the water content on the phase selectivity but also showing the difficulty in crystallizing pure silica Nu-87.

Table 2 Chemical composition of pure silica zeolites prepared with M_8BQ^{2+} as SDA

	g/100 g				
Zeolite	N	C	H	F	Unit cell composition
ZSM-12	0.783	7.306	1.189	1.071	$[(C_{22}H_{42}N_2)_{1.05}F_{2.08}][SiO_2]_{56}$
Beta	1.597	14.868	2.436	2.162	$[(C_{22}H_{42}N_2)_{2.78}F_{5.54}][SiO_2]_{64}$

Table 3 Zeolite synthesis results for aluminosilicate compositions using M_8BQ^{2+} as SDA[a]

H_2O/SiO_2	Al/(Al + Si)[b]	Time/days	Product
15	0.038	10	Amorphous
		17	Nu-87
15	0.020	7	Nu-87
		15	Nu-87
		28	Nu-87
15	0.012	13	Nu-87
		20	Nu-87
15	0.005	4	Nu-87
		7	Nu-87
15	0.000	7	ZSM-12
		14	ZSM-12
15[c]	0.000	1	ZSM-12
		3	ZSM-12
12.5	0.000	3	Beta
		14	Beta
		28	Beta + ZSM-12

[a]Crystallization temperature: 175 °C. The numbers in parentheses correspond to the crystallization time in days. [b]In the reaction mixture. [c]As-made Nu-87 used as seeds (5%)

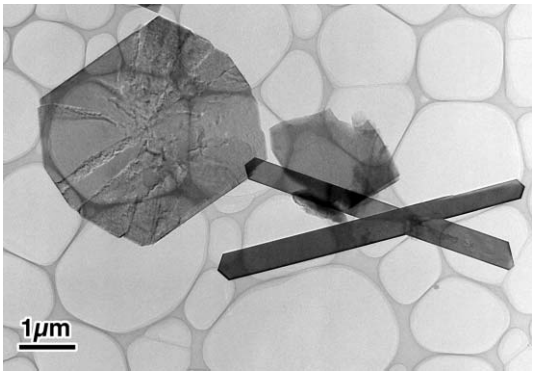

Fig. 1 TEM image of an aluminosilicate sample synthesized with M_8BQ^{2+}. According to powder XRD only Nu-87 (large flat platelets in the TEM picture) was registered. The TEM image demonstrates the coexistence in the product of some ZSM-5 impurity (elongated prisms).

We shall note here that, although ZSM-5 was not detected by XRD in the syntheses using M_8BQ^{2+}, electron microscopy revealed its presence in a synthesis in the presence of Al which yielded Nu-87 as the major phase (Fig. 1). Arguably, the minor crystallization of ZSM-5 with this cation may be due to a partial decomposition of the cation. As discussed below, the separation between the quinuclidine moieties in this diquat is probably not adequate for their location in ZSM-5 in adjacent intersections of channels.

M_6BQ^{2+} as SDA

For pure silica compositions we observe the same trends when the chain joining both quinuclidinium moieties contains 6 and 8 methylenes, with the only exception that with 6 methylene groups ZSM-5 (MFI) competes with Beta or ZSM-12 for H_2O/SiO_2 ratios of 10 or 15 (Table 4). The crystallization of ZSM-5 using this cation is not surprising given that its synthesis has been described also with other SDA diquats wherein the charged nitrogen atoms are separated by a chain of 6 methylenes.[19] As in those cases, we can imagine here a situation with each quinuclidinium group located at channel intersections in MFI while the methylene chain resides in the channel. Because of its intermediate length, a chain of 6 methylenes would fit better than a chain of 4 or 8 methylenes within this arrangement in MFI, which may explain why ZSM-5 may crystallize with M_6BQ^{2+} but we never observed it as a major phase with M_8BQ^{2+} or M_4BQ^{2+} (see below).

When Al is introduced into the synthesis gel (Table 5), we obtained at 175 °C the same three phases (ZSM-12, ZSM-5 and Beta) obtained in its absence. Actually, the trend is the one we typically observe,[4] *i.e.*, the phase selectivity effect when increasing the Al content is the same as the effect of decreasing the water content. Here, no Nu-87 was obtained, again suggesting the importance of the length of the methylene chain in determining the phase selectivity of the crystallization. Similar results were found using $(CH_3)_3N^+(CH_2)_n{}^+N(CH_3)_3$ linear diquats in hydroxide media, where diquats with $n =$ 5–12, 14 or 16 were tested but yielded Nu-87 only for

Table 4 Zeolite synthesis results for pure silica compositions using M_6BQ^{2+} as SDA[a]

	Temperature/°C		
H_2O/SiO_2	175	150	135
1.5	Beta + unknown (2)	unknown + Beta (6)	unknown (15)
	Beta (5)	Beta + unknown (15	unknown (28)
7.5	Beta (4)	am. + Beta (4)	am. + Beta (11)
	Beta (7)	Beta (11)	Beta (22)
10	Beta (7)		
	ZSM-5 + Beta (34)		
15	ZSM-12 + am. (4)	am. + ZSM-12 (8)	am. (19)
	ZSM-12 (11)	ZSM-12 + ZSM-5 (19)	Beta + ZSM-5 + am. (42)

[a]The numbers in parentheses correspond to the crystallization time in days; am. = amorphous solid, unknown = unidentified, unstable material with ill-defined XRD pattern (see ESI[†]).

Table 5 Zeolite synthesis results for aluminosilicate compositions using M_6BQ^{2+} as SDA[a]

Al/(Al + Si)[b]	Time/days	Product
0.038	7	Beta
	34	Beta + ZSM-5
0.020	7	ZSM-5 + Beta
	9	ZSM-5↑ + Beta ↓
0.000	4	ZSM-12 + am.
	11	ZSM-12

[a]Crystallization temperature: 175 °C. am. = amorphous solid. [b]In the reaction mixture.

$n = 10$[6] (although we note that the original patent shows also some examples of the synthesis of Nu-87 using diquats with $n = 8$ and 12, although $n = 10$ appears to work better).[17]

M_4BQ^{2+} as SDA

When the number of methylenes in the chain is further reduced to 4, new phase selectivity effects appear (Table 6). Here ZSM-12 is again the dominant phase for pure silica compositions at relatively high H_2O/SiO_2 ratios. However, as the concentration of the crystallizing mixture increases three new phases appear: ITQ-14 for intermediate concentrations and ITQ-8 and ITQ-10[20] for higher concentrations. We will show below that ITQ-14 is related to zeolite Beta and it actually appears at a similar crystallization field. ITQ-8, which is most likely a layered phase (see below) and ITQ-10 (a zeolite with an intergrown structure possibly related to the Beta family too) compete and undergo Ostwald ripening transformations at the lowest H_2O/SiO_2 ratios. Here there is once again an apparent contradiction in the sense of the Ostwald ripening transformations: from ITQ-8 to ITQ-10 to Beta at 175 °C and from ITQ-10 to ITQ-8 to Beta at 150 °C. These phase sequences were observed in repeated experiments. Nonetheless, it is possible to obtain both ITQ-8 and ITQ-10 as pure phases.

When Al is introduced into the synthesis mixture, we never obtained ITQ-14. ITQ-10 can be obtained for Si/Al ratios up to 25 but zeolite Beta is the phase obtained for Si/Al = 10 (Table 7). Using the same SDA but in hydroxide media, Lobo *et al.* only observed phase selectivity changes depending on the introduction of Al.[2] For pure silica compositions they observed the crystallization of ZSM-12, while Beta crystallized in the presence of aluminum.

Characterization

A number of techniques have been used to characterize the pure phases obtained during this study that present interesting features from the viewpoint of XRD (ITQ-8, ITQ-10, ITQ-14) or chemical composition (Nu-87).

Nu-87

The chemical composition of Nu-87 samples prepared with different Si/Al ratios is presented in Table 8. The C/N ratios are always close to the value in M_8BQ^{2+} (11), suggesting the integrity of the diquat in the zeolite. The Si/Al ratios in the zeolites are always smaller than in the crystallizing mixture, but

Table 7 Zeolite synthesis results for aluminosilicate compositions using M_4BQ^{2+} as SDA[a]

Al/(Al + Si)[b]	Time/days	Product
0.091	7	Beta
	14	Beta
0.038	7	ITQ-10
	14	ITQ-10
0.020	4	ITQ-10 + ITQ-8
	11	ITQ-10
0.000	2.5	ITQ-8
	4	ITQ-10
	10	ITQ-10 + Beta

[a]Crystallization temperature: 175 °C. The numbers in parentheses correspond to the crystallization time in days. [b]In the reaction mixture.

Table 6 Zeolite synthesis results for pure silica compositions using M_4BQ^{2+} as SDA[a]

	Temperature/°C		
H_2O/SiO_2	175	150	135
3.5	ITQ-8 + am. (1.5)		
	ITQ-8 (2.5)		
	ITQ-8 + ITQ-10 (3.5)	ITQ-10 + am. (4)	
	ITQ-10 (4)	ITQ-8 (10)	ITQ-10 + ITQ-8 + am. (10)
	ITQ-10 + Beta (10)	ITQ-8 + Beta (14)	ITQ-10 + ITQ-8 + am. (17)
7.5	ITQ-14 + am. (4)	ITQ-14 (12)	Beta + ITQ-10 (25)
	ITQ-14 (12)	ITQ-14 + ZSM-12 (25)	Beta + ITQ-10 (32)
15	ZSM-12 (3)	ZSM-12 (8)	ZSM-12 + am. (9)
	ZSM-12 (14)	ZSM-12 (16)	ZSM-12 (17)

[a]The numbers in parentheses correspond to the crystallization time in days.

Table 8 Chemical composition of Nu-87 zeolites prepared in fluoride medium using M_8BQ^{2+} as an SDA

Si/Al ratio		g per 100 g of zeolite						Contents per unit cell[b]		
Starting mixture	Zeolite	N	C	H	F	Residue[a] (wt%)	C/N	M_8BQ^{2+}	F	Al
25	20	1.18	11.15	1.88	—[c]	85.0	11.0	2.0	—[c]	3.4
50	33	1.20	11.18	1.84	0.32	84.9	10.9	2.1	0.8	2.1
50	41	1.19	11.28	1.89	—[c]	84.9	11.1	2.0	—[c]	1.7
80	60	1.18	11.04	1.86	0.36	84.7	10.9	2.0	0.9	1.1
200	170	1.12	10.62	1.92	0.48	84.4	11.1	1.9	1.2	0.4

[a]Percentage of mass remaining after thermogravimetric analysis in an air flow (800 °C). [b]There are 68 tetrahedral (Si or Al) atoms per unit cell in the NES topology. [c]Not measured.

it is possible to obtain Si/Al ratios of up to 200. It is worth noting that, very atypically, the fluoride content appears to show only a slight depence on the Al content, increasing from 0.8 to 1.2 F/uc when the Al content decreases from 2.1 to 0.4 Al/uc. This implies that as the Al content decreases the concentration of connectivity defects should increase and the fraction of positive charges of M_8BQ^{2+} counterbalanced by $Si–O^-$ groups should increase. Perhaps the reason for the difficulty in synthesizing pure silica Nu-87 using this SDA is thus related to the need of a too large concentration of connectivity defects, making the crystallites unstable in the crystallizing medium.[4]

ITQ-8

This phase could not be recognized either as a known zeolite or as any other phase in the JCPDS database. Its crystallites are typically ill-faceted and relatively small, being between 1 and 0.5 μm in two directions and around 0.2 μm in the third one. By TGA in air it is observed an exceedingly large weight loss of over 40%, which occurs chiefly in three steps: below 200 °C (a steady weight loss of *ca.* 10%), around 280–300 °C (abrupt weight loss of *ca.* 10%, accompanied by a sharp exothermic peak) and between 300 and 650 °C (*ca.* 20%).

As-made ITQ-8 is well crystallized (Fig. 2) and could be indexed in space group $P2_1/c$ with cell dimensions of $a = 17.325$ Å, $b = 13.422$ Å, $c = 16.107$ Å and $\beta = 99.605°$. A list of reflection positions and their indices is shown in Table 9. However, when the material is calcined in air to remove the occluded organics and fluoride its structure is destroyed, as judged from its XRD which only shows a reflection at 11.70 Å. *In situ* XRD during calcination in air shows that ITQ-8 is already much modified at 75 °C, and above 225 °C shows, esentially, the single reflection mentioned above (irreversibly shifted to smaller *d*-spacings as the temperature increases to 675 °C). This is about the same temperature range at which the second weight loss step proccess occurs, the exothermicity of which suggests this is the main step in the burning out of the occluded SDA. Thus, it appears that

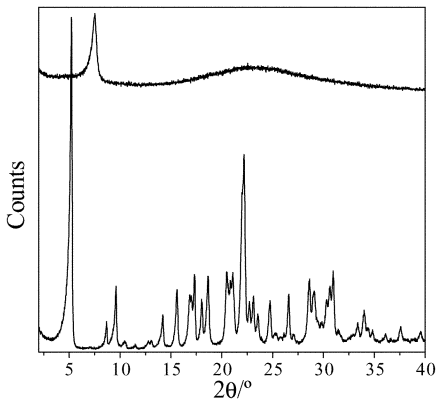

Fig. 2 XRD patterns of the as-made (bottom) and calcined (top) TQ-8.

Table 9 Reflection positions and indices for as-made pure silica ITQ-8 ($P2_1/c$, $a = 17.325$ Å, $b = 13.422$ Å, $c = 16.107$ Å, $\beta = 99.605°$)

2θ/°	h,k,l	2θ/°	h,k,l	2θ/°	h,k,l
5.17	1,0,0	16.95	3,1,−1	22.68	2,3,−1
8.63	0,1,1	17.29	0,2,2	23.07	2,0,−4
9.56	1,1,−1	18.04	0,1,3	23.53	2,3,1
10.35	2,0,0	18.63	3,1,1	24.69	4,2,0
10.52	1,1,1	20.44	3,2,0	25.24	4,0,2
11.46	1,0,−2	20.63	3,0,2	25.83	1,2,−4
12.74	2,1,−1	20.80	4,0,0	26.08	5,0,0
13.05	1,0,2	21.03	1,3,−1	26.55	0,4,0
14.17	1,2,0	21.15	2,2,2	27.06	1,4,0
15.55	3,0,0	21.94	3,1,−3		
16.77	2,2,0	22.15	2,1,3		

the occluded SDA is holding the structure together and its removal results in a major structural collapse. After calcination in air at 580 °C the material has a BET surface area of 150 $m^2\ g^{-1}$ and a micropore volume of 0.02 $cm^3\ g^{-1}$.

These observations suggest ITQ-8 could be a layered material but it could also be an interrupted framework, and the presence of a reflection remaining in the calcined material prompted us to check its stability and phase transformations by calcination under different conditions. Thus, as-made ITQ-8 was calcined in vacuum and its XRD was recorded *in situ* (Fig. 3). Even at room temperature the XRD pattern changes

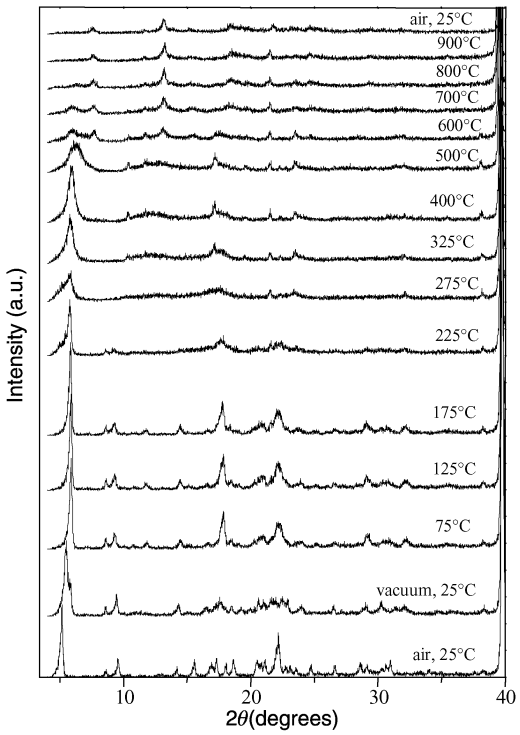

Fig. 3 XRD patterns of ITQ-8 recorded during *in situ* heating under vacuum.

Table 10 Chemical composition of two as-made samples of pure silica ITQ-8 synthesized with M_4BQ^{2+} $(C_{18}H_{34}N_2)^{2+}$

g per 100 g of solid					Molar ratios		
N	C	H	F	Residue[a] (wt%)	C/N	F/N	H/N
3.05	23.97	5.18	2.34	56.3	9.2	0.56	23.6
3.07	23.65	5.14	2.29	54.8	9.0	0.55	23.3

[a]Percentage of mass remaining after thermogravimetric analysis in an air flow (800 °C).

significantly as a consequence of the vacuum treatment. As the temperature increases changes are more dramatic, although up to 175 °C we can still recognize several of the reflections of as-made ITQ-8 (together with other very broad peaks). Above 700 °C a completely different XRD pattern, with only few weak and broad reflections is observed. Although this shows ITQ-8 may transform to a crystalline phase under careful calcination conditions, the crystallinity of the calcined material shown in Fig. 3 is too low to warrant a thorough characterization.

The chemical analysis of as-made ITQ-8 (Table 10) shows that most of the weight loss observed in the TGA experiments corresponds to organics (around 30 g per 100 g of as-made solid). The C/N ratio close to that in M_4BQ^{2+} (9) suggests most of the occluded SDA is intact. The remainder of the occluded material is 2.3% fluoride and around 13% water, as shown by the C/H ratio of over 23, much larger than that in M_4BQ^{2+} (17). This water should correspond actually to both occluded water and connectivity defects annealed during the high temperature treatments of the elemental analysis procedure. $Si–O^-$ groups in as-made ITQ-8 are necessary given that the amount of fluoride found in the material can counterbalance only half of the organic charges.

The ^{29}Si MAS NMR spectrum of as-made ITQ-8 is shown in Fig. 4. There is an intense and broad band centered around −100 ppm, assigned to Q_3 species (either $Si–O^-$ or Si–OH species) and at least three sharp resonances assignable to Q_4 species ($Si(OSi)_4$). A very small and broad band around −90 ppm can be assigned to Q_2 species. After deconvolution of the spectrum it is seen that the ratio of unconnected ($Q_3 + Q_2$) to fully connected (Q_4) species is 1 : 1. There are two Q_3 resonances of equal intensity (plus a smaller one) and four Q_4 resonances with relative intensities of 1 : 3 : 2 : 4.

The high resolution of the spectrum in the region of resonance of Q_4 species suggests a very high degree of local order in as-made ITQ-8 which implies that connectivity defects are not randomly distributed but occur in well defined crystallographic positions. All the observations for ITQ-8 suggest the as-made form is a layered material, possibly formed by the ordered array of silicate sheets separated and held together by layers of M_8BQ^{2+}. This is the case for RUB-18, for which the $Q_3 : Q_4$ ratio is also 1 : 1.[21]

ITQ-10

The XRD patterns of as-made and calcined ITQ-10 are shown in Fig. 5. Both consist only of very broad bands, suggesting the structure of ITQ-10 to be an intergrowth of different polymorphs (although we can expect also a contribution of the very small crystallite size, see below, to the peak broadening). The patterns closely resemble those of as-made and calcined zeolite Beta, which is also an intergrown structure.[22] However, there are clear differences, especially in the low angle region (very sensitive to the intergrowth pattern) where the presence of two broad reflections at 2θ 7.5 and 9° in ITQ-10 distinguish this material from zeolite Beta. There are also obvious differences in the 20–25° region: a sharp band at around 21.5° in zeolite Beta is absent in ITQ-10; the most intense reflection is much broader in ITQ-10 than in Beta (although this could also be due to the small crystal size of ITQ-10); there is a broad band around 24.2° in ITQ-10 that do not appear in Beta; and finally, a characteristic of calcined zeolite Beta is the presence of a sharp reflection at around 13.5° which is not found in ITQ-10 either before or after calcination.

The chemical analysis results of as-made ITQ-10 are given in Table 11. The C/N ratio is close to the value in M_4BQ^{2+} (9), suggesting the SDA is occluded esentially intact in this material. For pure silica compositions the fluoride content may counterbalance only around 90% of the organic charges, suggesting the presence of connectivity defects in ITQ-10. As the Al content increases the fluoride content decreases, suggesting the incorporation of Al as tetrahedral $[AlO_{4/2}]^-$

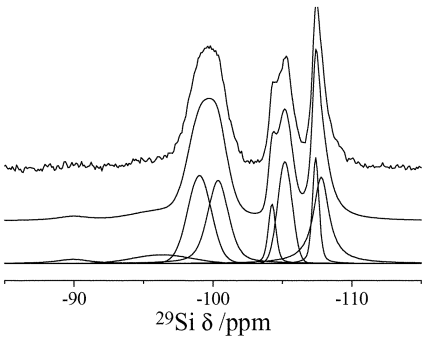

Fig. 4 ^{29}Si MAS NMR of as made pure silica ITQ-8 (from top to bottom): experimental, simulation and deconvoluted components.

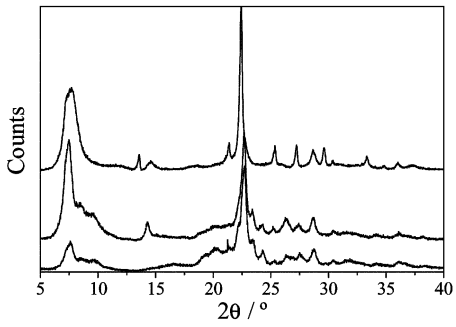

Fig. 5 XRD patterns of (from bottom to top) as-made and calcined pure silica ITQ-10 and calcined pure silica Beta prepared with the same SDA (M_4BQ^{2+}).

Table 11 Chemical composition of as-made ITQ-10 zeolites synthesized with M_4BQ^{2+} $(C_{18}H_{34}N_2)^{2+}$

Al/(Si + Al)		g per 100 g of zeolite					Molar ratios		
In starting mixture	In zeolite	N	C	H	F	Residue[a] (wt%)	C/N	F/N	(F + Al)/N
0.00		1.65	12.84	2.19	1.93	81.2	9.1	0.86	0.86
0.00		1.72	13.45	2.25	2.03	80.8	9.1	0.87	0.87
0.02	0.02	1.78	13.47	2.31	1.67	79.5	8.9	0.69	0.89
0.04	0.04	1.78	13.59	2.31	1.16	77.3	8.9	0.48	0.92

[a]Percentage of mass remaining after thermogravimetric analysis in an air flow (800 °C).

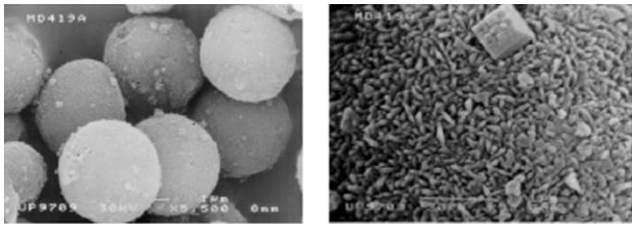

Fig. 6 SEM images of pure silica ITQ-10. The round aggregates shown in the left panel are composed of very small crystallites in the nanoscale range (shown in the right panel together with a crystal of zeolite Beta).

sites in the framework. The (F + Al)/N ratio is always below 1 and a certain concentration of connectivity defects is in all cases necessary to accomplish full charge balance. The weight of occluded organics is around 16–18%, while the whole weight loss in air at 950 °C is around 19–22% (accounting not only for organics but also for fluoride and water removal arising from dehydroxilation reactions).

Low magnification TEM shows that the crystallites of ITQ-10 appear as very small ellongated rods (around 0.2 μm long and 100 nm wide) aggregated in spheres of 2–5 μm (Fig. 6). While it is typically believed and generally found that the fluoride route yields large crystallites, although sometimes it can also produce crystals in the nanocrystalline range as the case shown in Fig. 6. We have found several other cases of nanocrystalline zeolites produced in fluoride media.[23] The competing crystallization of zeolite Beta in certain conditions (see above) may be evidenced by SEM even when no indication is found by XRD, as shown by the presence of isolated tetragonal bipyramids ended by pinacoids, frequently found for zeolite Beta produced in fluoride medium[24] (Fig. 6).

The ^{29}Si MAS NMR spectrum of calcined pure silica ITQ-10 (Fig. 7) shows a small and broad band around −100 ppm, assigned to Q_3 species, amounting to 2.3% of the total Si. The main intensity is in the region of resonance of Q_4 species and shows an extremelly low resolution, very atypical of pure silica materials prepared in fluoride media (see Fig. 11 in ref. 4) and in significant contrast to the typical spectrum of pure silica Beta (also shown in Fig. 7). The low resolution of Q_4 resonances for this relatively low concentration of defects suggests a low degree of short range order that could possibly be due to an intergrown structure consisting of very small domains. This would also be consistent with the observed XRD pattern, showing only very broad reflections.

The infrared spectra of as-made and calcined ITQ-10 are compared to that of calcined Beta in Fig. 8. Again, we observe broad bands and a poor resolution in ITQ-10 but also some similarity between the spectra of both materials in the 400–700 cm^{-1} range, a region that is very sensitive to the structure. In particular, the couple of bands at 575 and 523 cm^{-1},

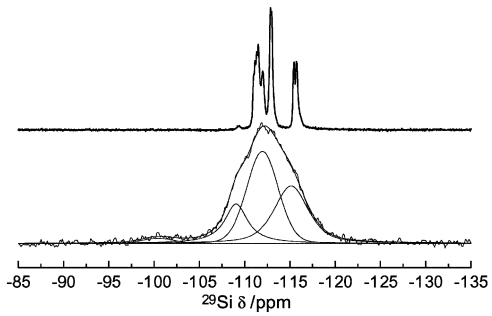

Fig. 7 ^{29}Si MAS NMR spectra of calcined pure silica ITQ-10 (from bottom to top: deconvoluted components, simulation and experimental traces) together with the spectrum of a standard pure silica Beta, shown for comparison (uppermost trace).

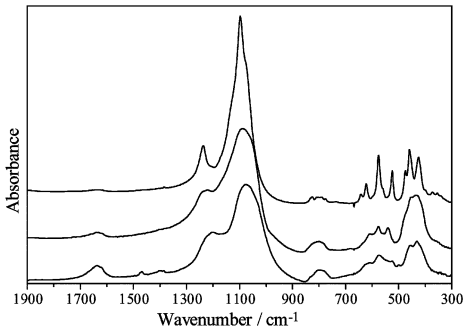

Fig. 8 Infrared spectra of pure silica zeolites (from bottom to top) as-made and calcined ITQ-10 and calcined Beta.

characteristic of Beta, appear at 575 and 537 cm^{-1} in calcined ITQ-10

As pointed out above, the decrease in the fluoride content as the Al content in ITQ-10 increases suggests that Al is being introduced into tetrahedral framework positions. Hence, after calcination to remove the organics, Al should give rise to Brønsted acidity by formation of Si–OH–Al bridges. The acidity in Al-containing ITQ-10 has been probed by infrared spectroscopy and pyridine adsorption. After outgassing at 400 °C under vacuum, the spectrum (Fig. 9) shows an intense band at 3745 cm^{-1}, assigned to free silanol groups, and a smaller band at 3610 cm^{-1}, characteristic of bridging OH groups. All these groups are acidic and accesible to pyridine, as they disappear upon pyridine adsorption and desorption at 250 °C (Fig. 10). In the region of scheletal vibrations of the adsorbed pyridine, the spectra after desorption at increasing temperatures (Fig. 10) show the existence of pyridine adsorbed on both Brønsted (band at 1545 cm^{-1}) and Lewis sites (1450 cm^{-1}). The intensity of the 1545 cm^{-1} band after desorption at 250 and 350 °C is essentially the same, while it decreases dramatically after desorption at 400 °C. This suggests that the bridging OH groups in ITQ-10 (Si/Al = 50) are of moderate acidity and all lie within a rather narrow distribution of acid strength. By contrast, the sample with a higher Al content (Si/Al = 25) shows only a very small band around 3610 cm^{-1}, and the intensity of the pyridinium band at 1545 cm^{-1} sharply decreases when the desorption temperature is increased from 250 to 350 °C (spectra not shown). This, and a large intensity of the 1450 cm^{-1} band (pyridine adsorbed on Lewis sites) suggests significant removal of framework Al upon calcination and a lower stability for the sample with high Al content.

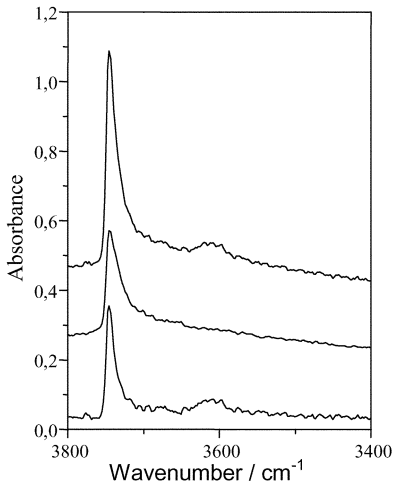

Fig. 9 IR spectra of calcined aluminosilicate ITQ-10 of Si/Al = 50 (from top to bottom): after outgassing at 400 °C under vacuum, after pyridine adsorption and the difference spectrum.

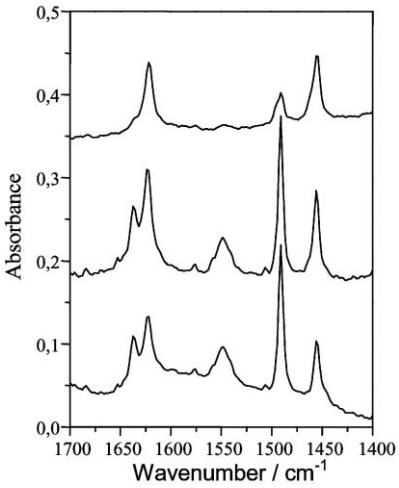

Fig. 10 IR spectra of aluminosilicate ITQ-10 (Si/Al = 50) after pyridine adsorption and outgassing at (from bottom to top) 250, 350 and 400 °C.

ITQ-10 is stable upon calcination at 580 °C in air (see Fig. 5 above). Its microporous properties were probed by N_2 adsorption which revealed a microporous volume of 0.18 $cm^3\ g^{-1}$ (derived by the *t*-plot method; 0.25 $cm^3\ g^{-1}$ measured at $P/P_0 = 0.4$) and a BET surface area of 488 $m^2\ g^{-1}$. The micropore volume is similar but just slightly smaller than that obtained for pure silica Beta (0.19 $cm^3\ g^{-1}$ by the *t*-plot method), although we note here that the effect of the crystal size on the microporous volume is not negligible in the nanocrystalline range,[25] as is the case for ITQ-10. The N_2 adsorption isotherm of ITQ-10 (not shown) is characteristic of a microporous solid with a very small crystal size, showing a steep plateau at intermediate pressures and a hysteresis loop at high relative pressures. We have also obtained the Ar adsorption isotherm of ITQ-10 and derived from it a pore size distribution using the Horvath–Kawazoe formalism. There is a single sharp peak centered at around 6.0 Å, suggesting ITQ-10 is a large pore zeolite. We must note, however, that this method of deriving approximate pore sizes is not very accurate and, when the channels open into large cages the method tends to give values larger than the crystallographic one.[26] It may be of value however to compare this result with those obtained for the large pore pure silica Beta, where a bimodal distribution with maxima at 5.6 and 6.8 Å was obtained,[27] or for the medium pore ZSM-5, with a maximum at 5.3 Å.

ITQ-14

The XRD patterns of as-made and calcined ITQ-14 are shown in Fig. 11. Again there is a large resemblance to zeolite Beta (and to ITQ-10), but the presence of a sharp reflection at around 10° (not shown by Beta and ITQ-10), a sharp reflection around 13.5° in the calcined material (present in calcined Beta but not in ITQ-10), a sharp reflection at 21.5° (present in Beta, not in ITQ-10) and a broad reflection at 24.2° (present in ITQ-10, absent in Beta) suggested to us that all these are related materials, consisting possibly of a different proportion or sequence of polymorphs.

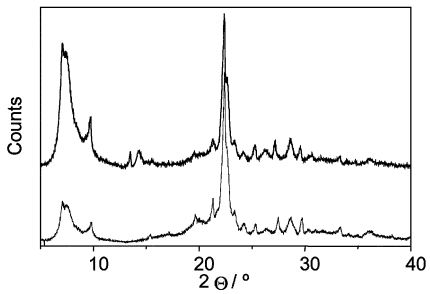

Fig. 11 XRD patterns of as-made (bottom) and calcined (top) pure silica ITQ-14.

Table 12 Chemical composition of two as-made samples of pure silica ITQ-14 synthesized with M_4BQ^{2+} $(C_{18}H_{34}N_2)^{2+}$

g per 100 g of solid				Residue[a]	Molar ratios		
N	C	H	F	(wt%)	C/N	F/N	H/N
1.71	13.37	2.20	—[b]	79.5	9.1	—[b]	17.9
1.72	13.51	2.29	1.37	79.8	9.2	0.59	18.5

[a]Percentage of mass remaining after thermogravimetric analysis in an air flow (800 °C). [b]Not measured.

The results of the elemental analysis of two samples of as-made ITQ-14 are shown in Table 12. The C/N ratio is close to that of M_4BQ^{2+} (9), suggesting the SDA is occluded intact within the pores of ITQ-14. The amount of organics is around 17 g per 100 g of zeolite and the amount of fluoride allows counterbalance of only 60% of the organic charges, suggesting the presence of connectivity defects in this material.

SEM micrographs of ITQ-14 reveal that the crystallites are relatively large, distinctly different from those of ITQ-10 and more like those of zeolite Beta, although the tetragonal bipyramids are not clearly distinguished. The micropore volume of ITQ-14 derived from the N_2 adsorption isotherms (0.19 $cm^3\ g^{-1}$ by the *t*-plot method, 0.24 at $P/P_0 = 0.4$) and the pore size distribution derived from the Ar isotherm (bimodal with maxima at 6.1 and 6.6 Å) suggests ITQ-14 is a three dimensional large pore zeolite.

The likelihood that ITQ-10 and ITQ-14 are 3D large pore zeolites possibly related to the zeolite Beta family of polymorphs together with the large concentration of F in D4R cages in ITQ-10 and ITQ-14 that we recently found,[13] prompted us to study both materials by HREM and electron diffraction. Unfortunately, ITQ-10 was too unstable under the beam to obtain definite structural conclusions, and the mere existence of channels was the only feature revealed by HREM in the extremelly small crystallite aggregates (Fig. 12). However, we could observe that ITQ-14 is a combination of "standard" beta zeolite crystallites with overgrown pillars, as shown in Fig. 13. Furthermore, by a new method combining electron diffraction and high resolution electronic microscopy we recently found[28] that those pillars have the structure of the hypothetical polymorph C proposed 13 years ago by Newsam *et al.*[22] In our opinion, the formation of polymorph C in this study is afforded by the use of fluoride anions during the synthesis. These anions may help stabilize the structure by their

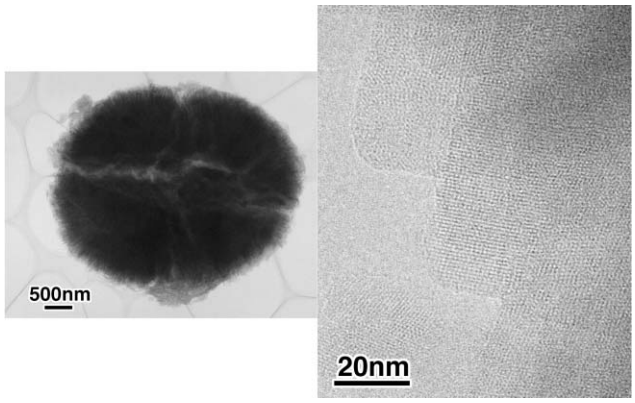

Fig. 12 TEM images of ITQ-10. The low resolution image shown left is of a globular particle composed of difuse components. The high resolution image shown right shows the presence of channels in this material.

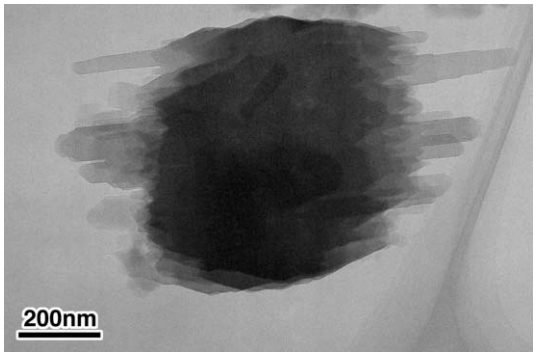

Fig. 13 TEM image of ITQ-14 showing elongated prisms overgrown on "standard Beta" zeolite. The elongated prisms have the structure proposed by Newsam *et al.* as a hypothetical structure of the beta family ("structure C").

inclusion in the D4R units which characterizes this structure. However, and given that structure C only appears as pillars overgrown on standard Beta, we should conclude that under these synthesis conditions structure C cannot nucleate but rather grows on other more readily formed polymorphs.

Conclusions

For all the three linear diquinuclidinium diquats tested (M_8BQ^{2+}, M_6BQ^{2+} and M_4BQ^{2+}) we have shown the influence of the degree of dilution of the synthesis mixture on the phase selectivity of the crystallization. The most frequently observed phases are the large pore zeolites ZSM-12 and Beta, of which the less dense phase (ZSM-12) appears under more dilute conditions, longer crystallization times and higher temperatures. The relative stability of both phases under the synthesis conditions is unclear.

When Al is introduced into the synthesis gel we generally found a similar effect on the phase selectivity as the effect of decreasing the water content, *i.e.*, the less dense phase is favoured when the Al content increases. There is however an important exception for M_8BQ^{2+}, for which a different phase (Nu-87 with high silica ratio) crystallized under conditions for which either ZSM-12 or Beta crystallize for pure silica compositions.

On the other hand, the importance of the length of the diquat is clear. The longest diquat (M_8BQ^{2+}) only yields two possible zeolites (Beta and ZSM-12) for pure silica compositions. By contrast, as the length of the methylene chain decreases the number of phases that crystallizes increases. ZSM-5 shows up under certain conditions using M_6BQ^{2+} (and only as an impurity with Mn_8BQ^{2+} and Al, possibly due to SDA decomposition). The crystallization of ZSM-5 only with this SDA is likely related to the separation of the quinuclidinium groups approximately matching the separation between adjacent channel intersections in the MFI structure. For M_4BQ^{2+} in addition to ZSM-12 and Beta three new phases crystallize: ITQ-8 (most likely a layered silicate consisting of silicate sheets held together by the organic cations), ITQ-10 and ITQ-14. The characterization of these two phases indicates that they are three-dimensional 12MR zeolites related to zeolite Beta. ITQ-14 is actually composed of pillars with the strcuture of the hitherto hypothetical structure C overgrown on standard zeolite Beta crystallites.

Acknowledgement

The authors acknowledge financial support by the Spanish CICYT (MAT 97-0723).

References

1 M. E. Davis and R. F. Lobo, *Chem. Mater.*, 1992, **4**, 756.
2 R. F. Lobo, S. I. Zones and M. E. Davis, *J. Inclusion Phenom. Mol. Recogn. Chem.*, 1995, **21**, 47.
3 H. Gies, *Stud. Surf. Sci. Catal.*, 1994, **85**, 295.
4 M. A. Camblor, L. A. Villaescusa and M. J. Díaz-Cabañas, *Top. Catal.*, 1999, **9**, 59.
5 J. L. Guth, H. Kessler, P. Caullet, J. Hazm, A. Merrouche and J. Patarin, in *Proc. 9th International Zeolite Conference*, ed. R. von Ballmoos, J. B. Higgins and M. M. J. Treacy, Butterworth-Heinemann, Boston, 1993, p. 215.
6 A. Moini, K. D. Schmitt, E. W. Valyocsik and R. F. Polomski, *Zeolites*, 1994, **14**, 504.
7 R. H. Daniels, G. T. Kerr and L. D. Rollmann, *J. Am. Chem. Soc.*, 1978, **100**, 3097.
8 M. E. Davis and C. Saldarriaga, *J. Chem. Soc., Chem. Commun.*, 1988, 920.
9 P. A. Barrett, E. T. Boix, M. A. Camblor, A. Corma, M. J. Díaz-Cabañas, S. Valencia and L. A. Villaescusa, in *Proccedings of the 12th International Zeolite Conference*, ed. M. M. J. Treacy, B. K. Marcus, M. E. Bisher and J. B. Higgins, Materials Research Society, Warrendale, PA, 1999, 1495.
10 J. L. Guth and R. Wey, *Bull. Soc. Fr. Minéral. Cristallogr.*, 1969, **92**, 105.
11 J. C. van der Waal, M. S. Rigutto and H. van Bekkum, *J. Chem. Soc., Chem. Commun.*, 1994, 1241.
12 M. A. Camblor, A. Croma and S. Valencia, *Chem. Commun.*, 1996, 2365.
13 M. A. Camblor, P. A. Barrett, M. J. Díaz-Cabañas, L. A. Villaescusa, M. Puche, T. Boix, E. Pérez and H. Koller, *Microporous Mesoporous Mater.*, 2001, **48**, 11.
14 L. A. Villaescusa, P. A. Barrett, M. Kalwei, H. Koller and M. A. Camblor, *Chem. Mater.*, 2001, **7**, 2332.
15 M. D. Shannon, J. L. Casci, P. A. Cox and S. J. Andrews, *Nature*, 1991, **353**, 417.
16 R. Gläser, R. Li, M. Hunger, S. Ernst and J. Weitkamp, *Catal. Lett.*, 1998, **50**, 141.
17 J. L. Casci and A. Stewart, *Eur. Pat.,* A-377291, 1990.
18 Y. Nakagawa, *US Pat.* 5,254,514, 1997; Y. Nakagawa, *World Pat.,*WO 97/06103, 1997.
19 L. W. Beck and M. E. Davis, *Microporous Mesoporous Mater.*, 1998, **22**, 107.
20 M. J. Díaz-Cabañas and M. A. Camblor, *Spanish Pat.*, P9901847, 1999.
21 S. Vortmann, J. Rius, S. Siegmann and H. Gies, *J. Phys. Chem. B*, 1997, **101**, 1292.
22 J. M. Newsam, M. M. J. Treacy, W. T. Koetsier and C. B. de Gruyter, *Proc. R. Soc. London A*, 1988, **420**, 375.
23 L. A. Villaescusa, *Ph.D. Thesis*, Universidad Politécnica de Valencia, 1999..
24 M. A. Camblor, A. Corma and S. Valencia, *J. Mater. Chem.*, 1998, **8**, 2137.
25 M. A. Camblor, A. Corma and S. Valencia, *Microporous Mesoporous Mater.*, 1998, **25**, 59.
26 M. J. Díaz-Cabañas, *Ph.D. Thesis*, Universidad Politécnica de Valencia, 1999.
27 S. Valencia, *Ph.D. Thesis*, Universidad politécnica de Valencia, 1997.
28 Z. Liu, T. Ohsuna, O. Terasaki, M. A. Camblor, M. J. Díaz-Cabañas and K. Hiraga, *J. Am. Chem. Soc.*, 2001, **123**, 5370.